Journal of Membrane Science 699 (2024) 122652

Contents lists available at ScienceDirect

Journal of Membrane Science

journal homepage: www.elsevier.com/locate/memsci

High gas permeance in CO_2-selective thin film composite membranes from bis(phenyl)fluorene-containing blends with PIM-1

Faiz Almansour [a,b], Andrew B. Foster [c], Ahmed W. Ameen [a,b], Sajjad Mohsenpour [a], Peter M. Budd [c], Patricia Gorgojo [a,d,e,*]

[a] Department of Chemical Engineering, The University of Manchester, Manchester, M13 9PL, UK
[b] Research & Development Center, Saudi Aramco, Dhahran 31311, Saudi Arabia
[c] Department of Chemistry, The University of Manchester, Manchester, M13 9PL, UK
[d] Instituto de Nanociencia y Materiales de Aragón (INMA) CSIC-Universidad de Zaragoza, C/ Mariano Esquillor s/n, 50018, Zaragoza, Spain
[e] Departamento de Ingeniería Química y Tecnologías del Medio Ambiente, Universidad de Zaragoza, C/ Pedro Cerbuna 12, 50009, Zaragoza, Spain

ARTICLE INFO

Keywords:
Bis(phenyl)fluorene
Cardo-PIM-1
CO_2 separation
PIM-1
Polymer aging
TFC membranes

ABSTRACT

A novel approach to improve the initial performance as well as to prevent physical aging of superglassy high free volume polymer PIM-1 is reported. Bis(phenyl)fluorene-based polymer of intrinsic microporosity (Cardo-PIM-1) was used at different loadings in PIM-1 to fabricate thin film composite (TFC) membranes and freestanding membranes. The gas performances of both TFCs and thick freestanding membranes exhibited similar trends; higher CO_2 permeance and higher CO_2/CH_4 selectivity at relatively low loadings ($\leq$5 wt %). TFCs containing 5 wt % Cardo-PIM-1 achieved a CO_2 permeance of (12600 $\pm$ 866 GPU), which corresponds to about a threefold increase as compared to the pristine TFC-PIM-1 membranes (2850 $\pm$ 254 GPU) and higher CO_2/CH_4 selectivity (14.6 $\pm$ 1.3) as compared to pure PIM-1 (10 $\pm$ 3). With regards to physical aging, PIM-1 TFC membranes experienced a 96 % reduction in CO_2 permeance after 1 year. However, for the TFCs containing 5 wt % cardo the reduction was considerably lower (59%) and all took place at an initial stage of up to 37 days, remaining at a good and stable CO_2 permeance of c.a. 5000 GPU for the remaining testing period of up to one year.

1. Introduction

Natural gas is the safest, cleanest, and most reliable fossil fuel source of energy [1]. Total global consumption of natural gas is around 95 trillion standard cubic feet per year [2], and the demand for natural gas will keep rising. However, natural gas reserves contain some undesirable contaminants such as hydrogen sulphide (H_2S) and carbon dioxide (CO_2). The presence of CO_2 in natural gas decreases its calorific value, causes pipeline erosion, and increases the volume of gas transported in the pipelines leading to a high cost of gas transportation [3,4]. Therefore, CO_2 removal is essential to achieve a clean fuel source and control atmospheric pollution. CO_2 level should be less than 2% to meet the strict specifications for natural gas transport so as to minimize corrosion [5].

Amine absorption is generally used for acid gas separations. However, this technology has several disadvantages, such as high capital and maintenance costs, high energy consumption and large carbon footprint. At present, membrane-based separation processes are being developed and implemented for natural gas sweetening, competing or in combination with existing technologies. The development and commercialization of membranes in industrial settings have gained interest over the years. This is due to the lower energy demand as compared to other technologies (directly translates into lower operating cost), easy scale-up, and smaller footprint [6]. However, only a few membranes are applied commercially for acid gas removal [2].

Traditional polymer membranes used for gas separation have relatively good chemical and thermal stability. However, they suffer from a permeability/selectivity trade-off as seen in the upper bound curves for several gas pairs plotted by Robeson [7], and they often undergo physical aging over time. Many polymers have been synthesized with enhanced gas separation properties. One of the most advanced classes of high free volume polymers are the polymers of intrinsic microporosity (PIMs) developed by Budd et al. [8]. The most descriptive member of this class is PIM-1, with pores of less than 2 nm, which arise as a result of

* Corresponding author. Departmento de Ingeniería Química y Tecnologías del Medio Ambiente, Universidad de Zaragoza, C/ Pedro Cerbuna 12, 50009, Zaragoza, Spain.
E-mail address: pgorgojo@unizar.es (P. Gorgojo).

https://doi.org/10.1016/j.memsci.2024.122652
Received 19 December 2023; Received in revised form 5 March 2024; Accepted 9 March 2024
Available online 11 March 2024

aromatic rings joined together forming a rigid ladder chain with spiro-centers acting as sites of contortion [9]. The unique rigid ladder structure restricts the movement of molecules, therefore inhibiting the packing of polymers and resulting in a high fractional free volume. PIM-1 has high CO_2 permeability and moderate selectivity towards this gas in conventional gas pairs such as CO_2/CH_4 or CO_2/N_2. PIM-1 is soluble in tetrahydrofuran, chloroform, and dichloromethane. It can be easily cast from solution to form solid membranes (i.e. it is solution-processable) [8]. All these properties make it suitable for membrane-based gas separation processes [10].

PIM-1 lies on the Robeson 2008 upper bound for certain gas pairs such as CO_2/CH_4 and CO_2/N_2 [11]. Like most glassy polymers, PIM-1 undergoes physical aging, i.e. the polymer becoming denser gradually as the polymer chains relax towards an equilibrium state [12]. Moreover, due to their higher free volume, PIMs age faster as compared to other glassy polymers [13,14]. The rate of physical aging depends on temperature [15], gas environment [16], structure of the polymer [17], and the thickness of the film (thin membranes age more rapidly) [18,19]. Therefore, studies have been carried out to explore ways of mitigating physical aging and enhancing their gas separation performance.

The movement of gas molecules through amorphous polymers is facilitated by the gaps or free volume between the polymer chains. This transport process is influenced by the thermal motion of the main polymer chain segments. In order to enhance the transport properties of these materials, efforts are made to enhance chain stiffness by adding rigid and bulky groups into the polymer chain. This, in turn, increases the free volume and impacts the packing density, subsequently improving selectivity and permeability [20]. Some studies have reported the effect of cardo polymers for gas separation processes [21–23]. A study by Kazama et al. [24] stated that bis(phenyl)fluorene-based cardo polymers with four phenyl rings connected to a quaternary carbon showed a restriction in the rotation of the phenyl groups. As compared to other commercial polymers, the cardo moiety restricts rotational movement and widens the average distance of the main chains, therefore higher gas permeabilities are obtained. Another study by Zhang [25] synthesized bis(phenyl)fluorene-based cardo diamine monomers with different side groups. The synthesized polyimides displayed a good selectivity towards hydrogen, due to the poor chain packing brought about by addition of bis(phenyl)fluorene cardo moiety and incorporation of CF_3 side groups into the polyimide backbones. Yahaya et al. [26] synthesized cardo-type random co-polyimide membranes for sour gas application. The membranes showed promising pure gas performance, CO_2 permeability of 323 barrer and CO_2/CH_4 selectivity of 35. Ghosh and Banerjee [27], studied the influence of cardo moiety in the poly(arylene ether)s (PAEs) on gas separation performance, the PAEs displayed a CO_2 permeability of 75 barrer and CO_2/CH_4 selectivity of 62. Camacho-Zuniga et al. [28] prepared membranes with cardo poly(aryl ether ketones), which displayed high glass transition temperature, outstanding thermal stability and CO_2 permeability of 72 barrer and CO_2/CH_4 selectivity of 25. These results were explained by chain packing and chain rigidity, demonstrating that reducing the length of the connector moieties between the cardo groups increased the fractional free volume, and the gas permeability. In another study by Carta et al. [29], cardo-polymers were synthesized using Troger's base polymerization reactions, the prepared adamantyl-based cardo-polymer showed good solubility, high molecular mass and a BET surface area of 615 $m^2\ g^{-1}$. The intrinsic microporosity of the polymer offered high gas permeabilities and moderate selectivities with certain gas pairs. In general, most of the reported cardo-containing polymeric membranes have good gas separation properties. This is due to the presence of the cardo moiety in the polymer matrix which restricts the packing of the chains and limits the rotational movement of the polymer backbone.

The first reported incorporation of a bis(phenyl)fluorene unit into a PIM structure was as part of copolymers prepared with bis(phenazyl)-based monomers [30]. One copolymer possessed good film forming properties, although the gas separation performance was not as good as PIM-1 (i.e. similar CO_2/CH_4 ideal selectivity but lower CO_2 permeability). Sun et al. [31] recently prepared a PIM structure based on a bis(phenyl)fluorene unit coupled with PIM-1 (Cardo-PIM-1) and prepared mixed matrix membranes (MMMs) by adding functionalized multi-walled carbon nanotubes (f-MWCNTs); 7.5 wt % loading led to an impressive CO_2 permeability of 29,000 barrer and a CO_2/N_2 separation factor of 24.2. The developed MMMs showed improved gas permeability due to enhanced gas solubility. However, aging behavior was not reported.

MMMs that contain inorganic particles often encounter difficulties including chain rigidification, poor interfaces and partial pore blockage, that consequently lowers their separation performance compared to what is theoretically projected. However, blending an organic polymer such as Cardo-PIM-1 with other polymers could potentially address the issues of low compatibility and thus improve separation performance [32]. Fabricating new materials and modifying existing ones can lead to membranes with enhanced separation performance. The polymer blend approach has been acknowledged as the most efficient and economically feasible among other methods. It combines the distinct advantages of different materials to form a new compound, with exceptional and synergistic properties that cannot be achieved through other synthetic methods [33].

Although the polymer blend method has unique advantages, it also comes with a number of drawbacks. One of the major drawbacks concerns their miscibility and homogeneity. Polymer blends can be classified into miscible, partially miscible and immiscible, depending on how well the components mix with each other. Miscible blends are two materials dissolved at the molecular level, resulting in a single phase, thus forming a homogenous system. In contrast, for immiscible blends the two components do not dissolve each other, therefore an interface is formed between two different phases. Partially miscible blends, or isotropic heterogenous materials, fall in between miscible and immiscible blends, where one component partially dissolves with the other component [33].

This paper reports the blending of a colloidal network-rich Cardo-PIM-1 into branched PIM-1 polymer matrices to form thin film composite (TFC) membranes and freestanding membranes. Their gas separation performance for the binary gas mixture CO_2/CH_4 is discussed, and the effect of different concentrations of Cardo-PIM-1 on their physical aging is also described. A range of characterization techniques were used to analyze the membrane's structural characteristics and their relation to gas separation performance.

2. Experimental

2.1. Materials

2,3,5,6-Tetrafluoroterephthalonitrile (TFTPN) was purchased from Fluorochem Limited (UK). Potassium carbonate (K_2CO_3) and dimethylformamide (DMF) were purchased from Fisher Scientific UK Ltd. 3,3,3′,3′-Tetramethyl-1,1′-spirobisindane-5,5′,6,6′-tetraol (TTSBI) was purchased from Alfa Aesar (UK). *N*,*N*-dimethylacetamide (DMAc), 1,2-dichlorobenzezne (DCB), dichloromethane (CH_2Cl_2), chloroform, toluene, acetone, 1,4 dioxane, methanol (≥99.5%), ethanol (≥99.5%), and 9,9-bis(3,4-dihydroxyphenyl) fluorene (BDPF) were purchased from Sigma-Aldrich (UK). TTSBI was dissolved in methanol and precipitated in dichloromethane before use. Polyacrylonitrile (PAN) supports with reference PS35 (thickness 165 μm, water flux 1600 L $m^{-2}\ h^{-1}\ bar^{-1}$, 97% rejection poly(ethylene glycol) of number-average molecular weight (M_n) = 20,000) were purchased from Sepro Membranes, Inc. (USA) and used for thin film membrane preparation. All the other chemicals were used as received.

2.2. Synthesis of PIM-1

PIM-1 was synthesized as described by Tamaddondar et al. [34] from monomers TTSBI and TFTPN as shown in Fig. 1. A clean 250 mL three-neck round bottom flask was dried overnight at 100 °C before use. An equimolar ratio of monomers TTSBI (10.20 g, 0.03 mol) and TFTPN (6.00 g, 0.03 mol), and K_2CO_3 (12.48 g, 0.09 mol) as a base, were added to the round bottom flask. The solid mixture was mechanically stirred at room temperature for 30 min under dry nitrogen flow. Then 60 mL of DMAc and 30 mL of DCB were added to the mixture. The mixture was stirred for another 30 min at room temperature under N_2 flow, to reach a homogenous mixture, and afterwards the temperature of the heater was set at 160 °C. 17 min were required to reach the set temperature. The flask was set up with a Dean-Stark trap to condense and collect water from the reaction mixture. The total time for the reaction, including the heating up to 160 °C, was 38 min. A hot, highly viscous solution was formed at the end of the reaction and was poured into 300 mL of methanol and then filtered by vacuum filtration using a sintered glass funnel. The product was dissolved in 300 mL of chloroform, re-precipitated in 900 mL of methanol, and then washed with deionized water under reflux at 95 °C overnight. Purification and solvent extraction of the solution was continued by washing the polymer with 200 mL of 1,4 dioxane, 400 mL of acetone, and then with 300 mL of methanol twice. Lastly, the purified PIM-1 was dried at 120 °C in a vacuum oven overnight and 12.73 g of PIM-1 were obtained (yield: 92%) as shown in Fig. S1 in the supporting information.

2.3. Synthesis of cardo-PIM-1

Cardo-PIM-1 was synthesized via the polycondensation reaction of three monomers following a procedure described by Sun et al. [31]. Monomers TFTPN (5.002 g, 25 mmol), TTSBI (4.25 g, 12.5 mmol) and BDPF (4.3795 g, 12.5 mmol), and K_2CO_3 (10.365 g, 75 mmol) were mixed in 150 mL of DMF. The mixture was mechanically stirred at 65 °C under N_2 flow for 72 h (Fig. 2). Once the mixture was cooled to room temperature, it was poured into 100 mL methanol, the crude product was vacuum-filtered using a sintered glass funnel, dissolved in CH_2Cl_2, and then re-precipitated in methanol to remove any insoluble materials. This procedure was repeated twice. Finally, the yellow solid filtrate was boiled in deionized water for at least 2 h and then dried in a vacuum oven at 80 °C for 2 days to obtain the Cardo-PIM-1 (yield: 90%).

2.4. Membrane fabrication

2.4.1. Thick freestanding membranes

In order to prepare freestanding membranes, 2 wt % of PIM-1 polymeric solutions with different loadings of Cardo-PIM-1 (1, 2, 5 and 10 wt%, percentages were calculated based on the mass of PIM-1) were used. The polymer mixtures were prepared by adding the required amounts of Cardo-PIM-1 into the polymeric solution (PIM-1 dissolved in chloroform), then subjected to probe sonication (UP200St (200 W, 26 kHz), Hielscher Ultrasound Technology, Germany) for 15 min in a pulsatile manner (5 s sonication with 3 s pause), followed by bath sonication for 2 h. After that, they were poured into Steriplan® Petri dishes (diameter of 5 cm) and immediately covered with a glass lid to slow down the rate of chloroform evaporation, and left to dry for 3 days at room temperature (shown in Fig. S2). The dried films were removed from the glass Petri dish, soaked in methanol for 8 h, and dried at 80 °C for 8 h under vacuum prior to gas permeation tests and characterization. The thickness of the membranes was measured by a micrometer (Mitutoyo IP65 Coolant Proof, United Kingdom, accuracy of 0.5 μm). The average membrane thickness resulted from at least 5 measurements on each membrane.

The prepared membranes were labelled *xxCardo-PIM-1,* where *xx* represents the wt.% of the Cardo-PIM-1 in the PIM-1 polymeric matrix.

2.4.2. Thin-film composite membranes

Thin film composite (TFC) membranes containing Cardo-PIM-1 supported on porous PAN substrates were prepared through kiss coating using the in-house built system that is shown in Fig. S3 in the supporting information. The polymer content used in all coating solutions was 2 wt% in chloroform, and the Cardo-PIM-1 loading ranged from 1 to 10 wt% relative to the polymer weight. The TFC solutions were subjected to probe sonication (UP200St (200 W, 26 kHz), Hielscher Ultrasound Technology, Germany) for 15 min in a pulsatile manner (5 s sonication with 3 s pause), followed by bath sonication for 2 h. PAN supports were cut into rectangular shapes (2.5 cm × 6 cm) and coated with the PIM-1 solution for about 0.7 s (Fig. S3). All membranes were dried at room temperature and atmospheric pressure and were labelled *TFC-xxCardo-PIM-1*, where *xx* represents the wt.% of Cardo-PIM-1. Pristine PIM-1 TFC membranes were labelled *TFC-PIM-1*.

2.5. Characterization and gas permeation measurement

2.5.1. Characterization of membranes and materials

A variety of characterization techniques were used to analyze the synthesized PIM-1 polymer powder, Cardo-PIM-1 polymer powder, TFCs and freestanding membranes.

A Viscotek gel permeation chromatography (GPC) max VE 2001 instrument (Malvern, UK) equipped with two PL mixed B columns and a Viscotek TDA302 triple detector array was used to determine the weight-average molecular weight (M_w), number-average molecular weight (M_n) and dispersity ($Đ_M = M_w/M_n$) of PIM-1 and Cardo-PIM-1. A polystyrene standard of known molar mass (110 kg mol^{-1}) was used for system calibration. PIM-1 and Cardo-PIM-1 were dissolved in chloroform at a concentration of 1 mg mL^{-1}. Each polymer solution was filtered through a 0.45 μm PTFE syringe filter prior to analysis. The analyses were performed in chloroform at a flow rate of 1 mL min^{-1} and an injection volume of 100 μL. OmniSEC software (Malvern, UK) was used to analyze the data, details of the instrument are as reported elsewhere [35].

Determination of network content: polymer solution in chloroform (1 mg mL^{-1}) was accurately prepared from 10 to 15 mg of a polymer sample. The entire solution was passed through 0.45 μm PTFE syringe filters and the exact weight of solution collected into a 30 mL sample bottle was recorded. The solvent in the bottle was allowed to slowly evaporate over several days. Once the solvent had visually completely evaporated, the bottle was placed in an oven at 100 °C to complete the drying process. The weight of polymer remaining in the bottle was measured and compared against the mass of filtered solvent (volume of chloroform) initially collected to determine the filtered polymer concentration. The network content by filtration was determined as the

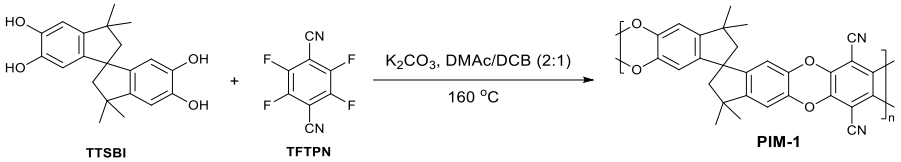

Fig. 1. Synthetic pathway of PIM-1.

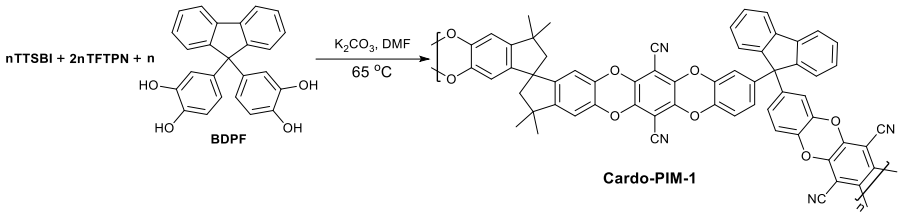

Fig. 2. Synthetic pathway of Cardo-PIM-1.

difference between the initial and filtered concentrations of the polymer as a percentage.

Dynamic light scattering (DLS) analysis of PIM-1 sample dispersions (50 ppm) in chloroform at 20 °C were completed on a Malvern Zetasizer Nano ZS instrument.

Proton nuclear magnetic resonance spectroscopy (^{1}H NMR) was performed using a Bruker DPX 400 MHz instrument for Cardo-PIM-1 and PIM-1 solutions in deuterated chloroform having a concentration of 0.05 g mL^{-1}.

The surface areas of PIM-1 and Cardo-PIM-1 were determined by Brunauer-Emmett-Teller (BET) analysis of the N_2 adsorption isotherm at 77 K, using a Micromeritics ASAP 2020 volumetric adsorption analyzer (Micromeritics, USA). Samples were first degassed under high vacuum at 120 °C for 12 h.

PIM-1, Cardo-PIM-1, thin film composite and freestanding membranes were studied using Attenuated Total Reflection Fourier transform infrared spectroscopy (ATR-FTIR). The spectra were acquired with an iDS Nicolet iS5 instrument (Thermo Scientific, UK), equipped with a Ge crystal as a background over the wavenumber range of 500–4000 cm^{-1}, and step size of 0.5 cm^{-1}.

Thermogravimetric analysis (TGA) was used to study the thermal stability of PIM-1, Cardo-PIM-1, TFCs and freestanding membranes. A TGA 550 thermal analyzer (TA Instruments, USA) was used, with a heating rate of 10 °C min^{-1} and under 60 mL min^{-1} nitrogen flow rate. The analyses were carried out from room temperature up to 700 °C.

Scanning electron microscope (SEM) FEI Quanta 650 FEG SEM (FEI, USA), was used to study the morphology of the TFC membranes. The cross-sectional samples were prepared by cryo-fracturing in liquid nitrogen. Initially, the membrane was immersed in ethanol for about 30 s, then in liquid nitrogen for another 30 s, where the membrane was fractured. Samples were sputtered with platinum nanoparticles using an Emitech sputter coater (Quorum Technologies, UK) before imaging.

X-ray diffraction (XRD) in the 2θ range 4 - 45° was carried out using a PANalytical X'pert Pro X'Celerator diffractometer with Cu-Kα radiation at a voltage of 40 kV and current of 40 mA. The lattice spacings (d) were obtained using Bragg's law Equation (1).

$$d = \frac{\lambda}{2\,sin\theta} \tag{1}$$

where, λ ($\lambda = 0.154$ nm) is the wavelength of the Cu Kα x-ray (nm) and θ (degree) is the diffraction angle.

Elemental analysis of PIM-1 and Cardo-PIM-1 was carried out using a Flash 2000 Organic Elemental Analyzer (Thermo Scientific, The Netherlands).

2.5.2. Gas permeation measurements

2.5.2.1. Thick freestanding membranes. Gas permeation measurements of freestanding membranes were obtained using a binary CO_2/CH_4 mixture with equal volume fractions of each gas at flow rates of 25 mL min^{-1} of each gas in a constant pressure system. The feed pressure was controlled at 2 bar, while the permeate side was kept at atmospheric pressure. Helium (flow rate of 20 mL min^{-1}) was used as a sweep gas to dilute the permeating gases and direct them to a 490 micro gas chromatography system (Agilent, USA) equipped with a PoraPLOT (PPU) column. The experiments were performed at 25 °C. Details of the gas separation unit used are reported elsewhere [36].

The gas permeability P_i for each gas was calculated using Equation (2).

$$P_i = \frac{Q_i\, l}{A\Delta p} \tag{2}$$

Where, Q_i is the permeate gas flow rate (cm^3 (STP) s^{-1}), $\boldsymbol{l}$ is the membrane thickness (cm), $\boldsymbol{A}$ is the effective membrane area (cm^2) and Δp is the gas partial pressure difference across the membrane (cmHg). P_i is calculated in barrer units (1 barrer = 10^{-10} cm^3 [STP] cm cm^{-2} s^{-1} cmHg^{-1}).

The selectivity for a gas pair, $\alpha_{A/B}$ (gases A and B) is calculated as the ratio of the permeabilities of the two gases, P_A and P_B, gas A being the most permeable of the two, using Equation (3).

$$\alpha_{A/B} = \frac{P_A}{P_B} \tag{3}$$

All membrane samples were sandwiched between two circular aluminum tapes and sealed with epoxy resin to avoid cracking and damage when handling and during testing. The effective membrane area ranged from 0.21 to 0.37 cm^2 as calculated by ImageJ software. At least two membranes of each composition were tested, and the average results along with standard deviation are reported.

To study the effect of the Cardo-PIM-1 in the fabricated membranes, single gas permeation measurements were investigated using a time-lag apparatus, which is a constant volume instrument, to evaluate the solubility (S) and diffusion (D) coefficients at a temperature of 25 °C and feed pressure of 1.2 bar. Firstly, both the permeate and the feed side of the membrane cell were vacuumed for 2 h using an Edwards T-station turbo pumping station 75 with an EXT75DX turbopump and an E2M1.5 rotary vane oil-sealed pump. On the permeate side, the initial pressure was 10^{-3} mbar and subsequent increments in pressure were measured by MKS baratron gauges at intervals of 1 s for 500 s and with an accuracy of 10^{-4} mbar. Data were collected using Labview and NI CRio. The permeability of a gas (P_i) was calculated using Equations (4) and (5). Details of the time lag apparatus are reported elsewhere [36].

$$Q_i = \frac{V_p\, v_{stp}}{RT} \times\ dp/dt \tag{4}$$

$$P_i = \frac{Q_i\ l}{A\ \Delta P} \times 10^{10} \tag{5}$$

Where, Q_i is the gas flow rate (cm^3 s^{-1}), V_p (cm^3) is the permeate side volume, v_{stp} is the molar volume of a gas at standard temperature and pressure (22400 cm^3 mol^{-1}), R is the gas constant (cmHg cm^3 K^{-1} mol^{-1}), T is the absolute temperature (K), dp/dt is the pressure build-up of permeate side (cmHg s^{-1}), Δp is the average pressure difference between feed and permeate sides (cmHg), and l is the membrane thickness (cm). The diffusion coefficient (D) was obtained using Equation (6). The solubility coefficient (S) was calculated from the permeability (P) and diffusion (D) coefficients using Equation (7); the time-lag (θ) was attained from the graph of permeate pressure against time.

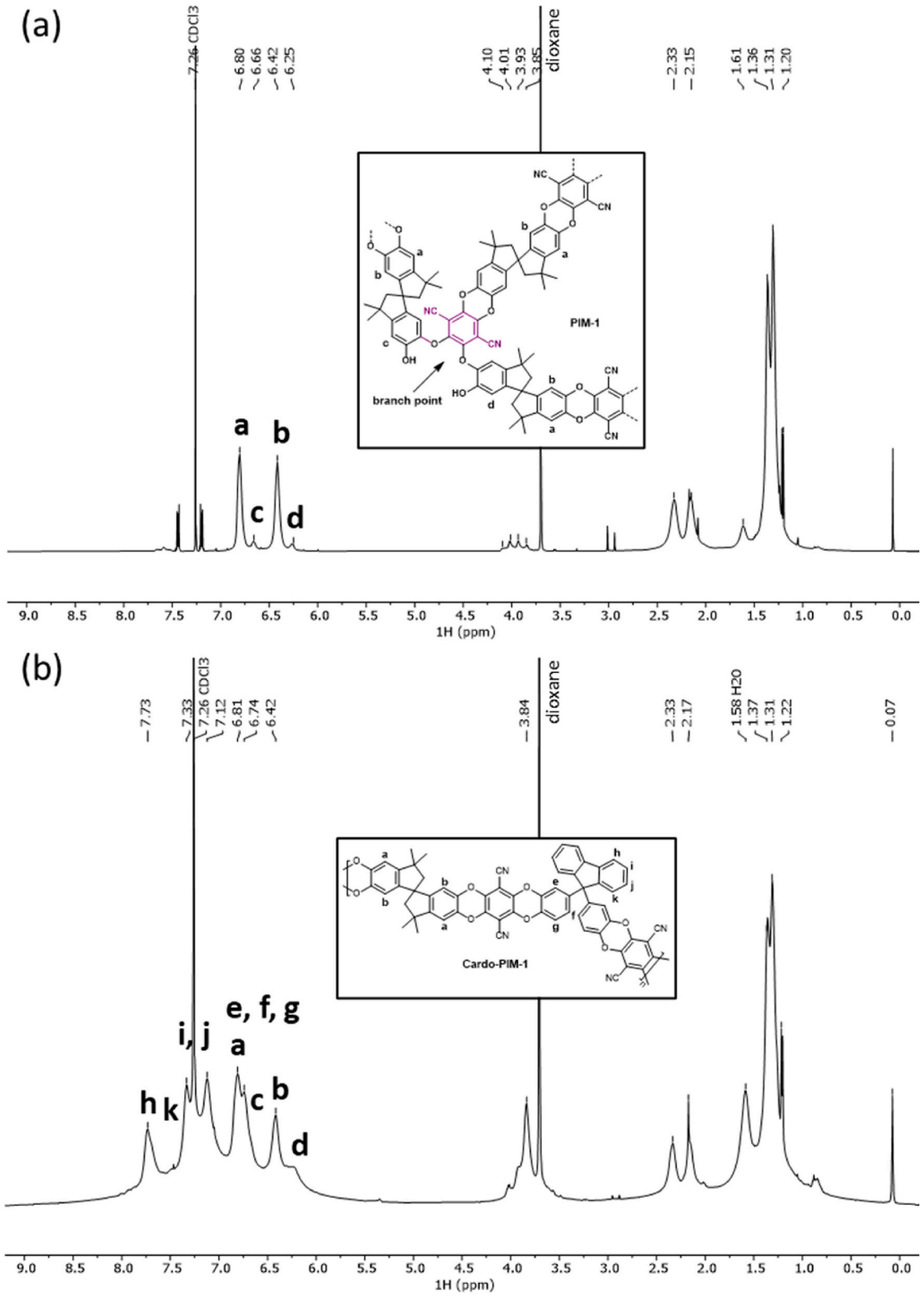

Fig. 3. Proton NMR spectra of PIM-1 (a) and Cardo-PIM-1 (b) polymers in CDCl3.

$$D = \frac{l^2}{6\theta} \quad (6)$$

$$P = DS \quad (7)$$

2.5.2.2. Thin-film composite membranes. Single gas (CO_2 and CH_4) permeation measurements were carried out based on the fixed pressure, standard variable volume method with a set up described elsewhere [37]. Pure gas permeation measurements were performed at room temperature with membrane effective area of 2.1 cm^2. Membranes were cut into coupons and directly mounted into the permeation cell. The pressure of the feed side was maintained at 2 bar and the permeate side was kept at atmospheric pressure. For aging studies, different coupons were tested but cut from the same rectangular membrane. At least two coupons from two different rectangular membranes were tested and the average permeance values were reported. The gas permeance is calculated in GPU (1 GPU = 10^{-6} cm^3 [STP] cm^{-2} s^{-1} $cmHg^{-1}$) according to Equation (8).

$$Permeance = 10^6 \times \frac{V_k}{t A \Delta p} \quad (8)$$

where, $\boldsymbol{V_k}$ (cm^3) is the volume of the permeated gas at STP (0 °C and 1 atm) during a time $\boldsymbol{t}$ (s) through a membrane area $\boldsymbol{A}$ (cm^2).

3. Results and discussion

3.1. Characterization of cardo-PIM-1, PIM-1, freestanding membranes, and TFCs

The weight-average molecular weight (M_w), number-average molecular weight (M_n), and dispersity ($Đ_M$) of PIM-1 and Cardo-PIM-1 were analyzed by multi detector GPC. PIM-1 exhibited M_w = 85000 g mol^{-1}, M_n = 42140 g mol^{-1}, and a $Đ_M$ of 2.0. The recovered Cardo-PIM-1 did not entirely dissolve in chloroform but proved to finely disperse in the solvent (cloudy solution), something previously observed with colloidal network rich PIM-1 polymer samples [38]. The soluble polymer portion of Cardo-PIM-1 showed M_w = 38500 g mol^{-1}, M_n = 6700 g mol^{-1}, and a $Đ_M$ of 5.7. Low sample recovery was observed during the GPC analysis and separate network content analysis indicated that the Cardo-PIM-1 contained approximately 70 % colloidal network content. DLS analysis indicated the presence of a polydisperse distribution of insoluble particles in chloroform (50 ppm). This combination of high colloidal network content and a lower molar mass distribution of remaining soluble polymer (much lower than that of PIM-1) meant that it was not possible to cast Cardo-PIM-1 as either a free-standing film or as a thin film composite, as can be observed in Fig. S4.

The ^{1}H NMR spectra of synthesized PIM-1 and Cardo-PIM-1 polymers are shown in Fig. 3(a) and (b), respectively. The PIM-1 polymer sample was more highly branched than typically expected from this synthetic procedure. We have recently reported how a marginally lower initial temperature ramp profile of high setpoint polymerizations (160 °C) can vastly increase the level of branching present in the polymeric structure [39]. This combined with insufficient nitrogen purging are the main factors which can result in higher than expected structural heterogeneity in a PIM-1 polymer sample. Extra peaks present in the aromatic region at 6.66 and 6.25 ppm are attributed to protons **c** and **d** in the branched structure presented in Fig. 3 [40]. The amount of branching residues present in the overall polymeric structure was determined at 11.7 % by comparing the integral areas of these two peaks to the two main aromatic proton peaks, **a** and **b**, associated with disubstituted residues found at 6.80 and 6.42 ppm respectively (Fig. S5) [39]. The other main broad peaks in the PIM-1 spectrum are associated with methylene (2.33 and 2.15 ppm) and methyl protons (1.3 ppm) from the cyclopentane ring section of the polymeric structure. Other significant peaks present are associated with residual water (1.61 ppm) and dioxane (3.71 ppm) remaining in the polymer sample. The proton NMR spectrum of Cardo-PIM-1 has added complexity in the aromatic region owing to the incorporation of the bis(phenyl)fluorene unit into the polymeric structure [31]. Resolved peaks above 7 ppm are attributed to pairs of aromatic protons, **h**, **i**, **j** and **k**. Aromatic protons, **e**, **f** and **g**, have similar local environments to the main aromatic protons associated with PIM-1 and are generally unresolved, except for an extra peak at 6.74 ppm. The presence of a partially resolved peak feature at around 6.25 ppm associated with aromatic proton, **d**, would indicate that this Cardo-PIM-1 polymer, like the PIM-1 polymer, has branching units within its structure. Both spectra contain broad peak resonances around 4 ppm which can be tentatively assigned to the unreacted hydroxy protons left behind on the formation of a branched unit.

Plots in Fig. S6 (a) and (b) show the N_2 adsorption/desorption isotherms of PIM-1 and Cardo-PIM-1, respectively, at 77 K. It can be observed that both polymers show high N_2 uptake at very low relative pressure, which confirms the microporous structure of the polymers. The BET surface area of PIM-1 is 657 m^2 g^{-1} and for Cardo-PIM-1 is 523 m^2 g^{-1}, which are all within the range of values reported in the literature [8,31,40]. Table S1 shows the elemental analysis for both PIM- 1 and Cardo-PIM-1. Results indicate lower values of carbon and nitrogen for the synthesized PIM-1 powder, which is lower than the ideal values of PIM-1. This could be due to the presence of residual solvents in the polymers [40].

The FTIR spectra of both PIM-1 and Cardo-PIM-1 (Fig. S7 (a)) show absorption peaks at 2242 cm^{-1}, which are associated with the nitrile (C ≡ N) stretching. In addition to that, characteristic bands such as aliphatic and aromatic C–H stretching (ca. 2840–3000 cm^{-1}), C═C aromatic bending (ca. 1620 cm^{-1}), and C–O stretching (ca. 1000–1400 cm^{-1}) are also present in the FTIR spectrum of PIM-1 and Cardo-PIM-1. Fig. S8 (a) and (b), show the FTIR spectra of the TFC and freestanding membranes, respectively. No additional peaks or shifts for bands are detected in the spectra of the TFCs and freestanding membranes as compared to the FTIR spectrum of pristine PIM-1 membranes. This might be due to the low Cardo-PIM-1 concentration of the prepared membranes.

The thermal stability of all polymeric materials was examined through TGA analysis (Fig. S7 (b)). Weight losses below 150 °C can be attributed to the loss of adsorbed solvents. In addition, samples of a freestanding PIM-1 membrane and pieces of the cracked film obtained when casting the Cardo-PIM-1 solution were tested and displayed high thermal stability up to approximately 480 °C owing to dipolar interaction in nitrile groups, which is in accordance with the literature data [20,24]. Similarly to pristine PIM-1 membranes, the thermal stability of the TFCs and freestanding membranes was also investigated and the results (Fig. S9 (a) and (b), respectively) indicate no significant differences for freestanding membranes, similarly to what was observed in a previous work [41]. However, we found differences in degradation behavior between TFCs cast from different blends (Fig. S9 (b)); TFCs with 5 and 10 wt% Cardo-PIM-1 show degradation temperatures that are c.a. 40 °C higher. This suggests strong intermolecular forces between polymer chains of the two polymers and increased miscibility. In this case, we have a colloidal polymer network structure interacting with a non-network branched polymer at polymer chain level such that some degradation profiles exceed in stability both of the two polymers when present individually. Synergies in overall polymer degradation of blends have been previously observed where semi interpenetrating polymer networks between two types of polymers form [42]. It is worth noting that the interactions which form during the rapid film formation of the TFCs are fixed for a considerable amount of time and influence the aging profile as discussed in section 3.2. By contrast, TGA profiles of self-standing blended films do not show up the same extent of differences in polymer degradation. The formation of a thick film is at the other extreme in terms of solvent evaporation; the film forms slowly on evaporation of solvent over 3–4 days so the nature of the interactions formed may be different initially and influence aging differently.

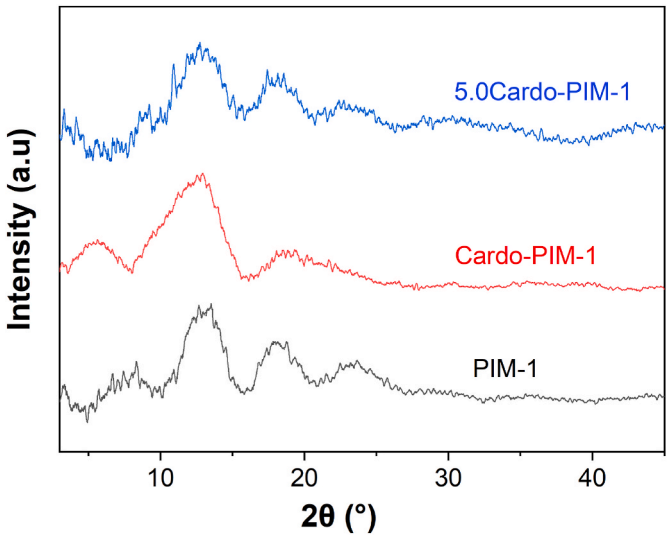

Fig. 4. XRD patterns of PIM-1 (powder), Cardo-PIM-1 (powder) and membrane 5.0Cardo-PIM-1.

Fig. 4 shows the XRD patterns of PIM-1 and Cardo-PIM-1 powder. The absence of sharp diffraction peaks indicates the amorphous structure of PIM-1 and Cardo-PIM-1. Characteristic broad peaks of PIM-1 appear at approximately 13°, 18°, and 23°, which is in agreement with data found in the literature [31]. The first two broad peaks centered at 13° and 18° are attributed to the micropores between loosely packed polymer chains, and chain to chain distance of the packed polymer, respectively, and the peak at 23° is representative of aromatic systems. The three peaks in the Cardo-PIM-1 are broader, which reveals a more inhomogeneous arrangement of the microporosity. In addition, a more evident peak at 5.5° suggests bigger micropores that can be explained by the more inefficient packing of the cardo polymer as a consequence of its more rigid and contorted architecture. The XRD spectrum of a membrane containing 5 wt% Cardo-PIM-1 is similar to that of PIM-1, but with a slightly broader peak at 13°, which suggests changes in spacing within the polymer blend.

Fig. 5 displays the SEM images of the surface and cross-sections of TFC-PIM-1 membranes and TFCs containing Cardo-PIM-1. As seen in the images, defect-free membranes with no agglomerates were produced using the kiss coating setup. Fig. S10 displays more cross-sectional images and additional surface micrographs. All thin membranes exhibited a thickness of about 1.5–2.5 μm and from a weight percent of Cardo-PIM-1 of 5 or higher the selective thin layer atop the support seems to be less dense than those at lower loadings or just pristine PIM-1. It is worth noting that in some of the images the PIM-1 layer seems to have detached from the porous support. However, this is due to the SEM sample preparation where the membranes are immersed in liquid N_2. The kiss-coating membrane preparation technique allows some intrusion of the coating polymer that leads to mechanical stability under ambient and gas testing conditions.

3.2. Gas separation results

Gas permeation tests of PIM-1 TFCs and TFCs containing Cardo-PIM-1 were carried out with single gases (CO_2, CH_4) on a fixed pressure cell at 25 °C. The CO_2 permeance and the ideal CO_2/CH_4 selectivity of the membranes are plotted in Fig. 6, and the raw data is provided in the supporting information (Table S2). The performance of these membranes was studied on days 1, 16, 22, 37 and 365 after preparation. The pristine PIM-1 TFC displays an average CO_2 permeance and CO_2/CH_4 selectivity of (2850 ± 254) GPU and (10 ± 3), respectively, which is similar to values previously reported by our group [43].

The nature and amount of Cardo-PIM-1 in the TFCs significantly impact their CO_2/CH_4 separation performance. A noteworthy increase in the CO_2 permeance of the PIM-1 TFC membranes was detected with increasing loading over the range 1–10 wt% of Cardo-PIM-1, reaching a maximum CO_2 permeance of (12632 ± 866) GPU for membrane TFC-5.0Cardo-PIM-1. This represents an increase of 343 % when compared to pristine TFC PIM-1 membranes. As reported by Sun et al. [31], this could be due to the fact the Cardo-PIM-1 can disturb the polymer packing due to the presence of the fused-ring in the Cardo-PIM-1 structure, leading to an increase in gas solubility. They also reported that Cardo-PIM-1 has higher fractional free volume (32.7%) compared with that of PIM-1 (29.4%), larger pore-size distribution than PIM-1, and higher CO_2 adsorption capacity over N_2. It is worth noting that the thickness of the selective PIM-1 layer is similar for all the TFCs and is in the range 1.4–1.7 μm (Fig. 5), and viscosity changes would not be so significant as to alter or increase penetration of the PIM-1 solution into the support during membrane formation. The trend of increased CO_2 permeance for the TFCs up to 5 wt% coincides with the trend of increased D and S for thick freestanding membranes (Table 1).

The permeance of CO_2 dropped for Cardo-PIM-1 loadings of 10 wt% as compared to the values achieved at 5, 2 and 1 wt%, but was still higher than that of pure PIM-1 membranes; the sample TFC-10.0Cardo-PIM-1 showed a CO_2 permeance of (4903 ± 131) GPU. This reduction might be due to polymer rigidification, i.e. lower mobility of polymer chains [44], nearby the phase separation, as suggested by the higher diffusivity selectivity in thick freestanding membranes; the diffusivity selectivity increased from 2.2 for PIM-1 to 2.9 for the 10Cardo-PIM-1 as seen in Table 1.

Regarding gas selectivity for the reported gas pair, the standard deviation values at each loading for the TFCs is relatively low in comparison with that for the purely PIM-1 TFC. For TFCs at 5 wt% Cardo-PIM-1 loading, the average CO_2/CH_4 selectivity increased due to good compatibility between the PIM-1 and the Cardo-PIM-1, i.e. absence of interfacial voids [45], and higher diffusivity and solubility selectivity values (as reported in Table 1 for freestanding membranes prepared with the same Cardo-PIM-1 loadings).

PIM-1, as all high free volume polymers, undergoes physical aging that causes a decrease in gas permeability over time, typically accompanied by an increase in selectivity. Physical aging refers to the loss of free volume of the polymer matrix through diffusion and simultaneous reorganization of the polymer chain packing in an attempt to reach a thermodynamic equilibrium state [16,19]. Aging over time in thin film membranes, typically used in industrial applications, is even more critical than that of freestanding ones, as loss of performance takes place faster for reduced thicknesses.

Membranes fabricated in this work were kept in plastic Petri dishes and sealed with parafilm throughout the aging period. The gas separation performance of these membranes was studied on days 1, 16, 22, 37 and 365 after preparation, and results are plotted in Fig. 7 (raw data is provided in the supporting information Table S2).

Fresh TFC membranes with PIM-1 as a selective layer showed a CO_2 permeance average value of 2850 ± 254 GPU. After 16 days, there was a significant drop in CO_2 permeance down to 1045 ± 140 GPU (63% drop in permeance) and improved CO_2/CH_4 selectivity from 10 ± 3 to 14 ± 1 (Fig. 7), which is mainly due to the rapid physical aging of the TFCs. After 37 days of aging, the CO_2/CH_4 selectivity increased by 41%, but 80% of the initial CO_2 permeance was lost. More so, after one year the CO_2 permeance loss was 96% (117 ± 12 GPU). Over the same period, the loss in CH_4 permeance was even higher (c.a. 99%) than that for CO_2, leading to an increase in the ideal selectivity for the CO_2/CH_4 mixture upon aging, which is an expected behaviour [46]. These results confirm typical physical aging behaviour of glassy polymers due to their non – equilibrium state after solvent removal, which is the state where molecules rearrange spontaneously and lattices contract towards equilibrium at temperatures below the glass transition temperatures, resulting in an increase in gas pair selectivity and a decrease in free volume and permeability [17].

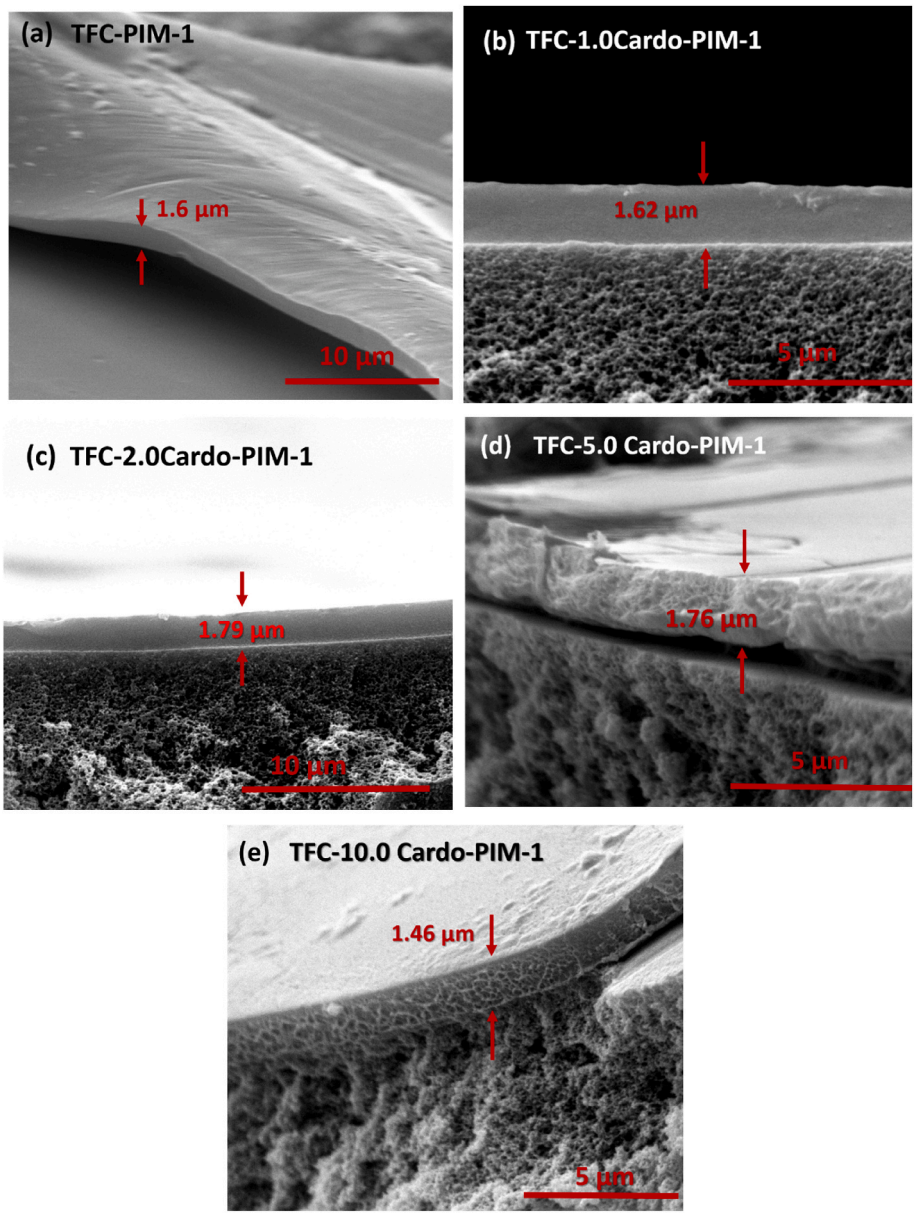

Fig. 5. SEM images of cross sections of TFC-PIM-1 (a) and TFC membranes containing different loadings of Cardo-PIM-1 (b–e).

Bernardo et al. [16], reported that aging in PIM-1 membranes mostly affects their gas diffusivity, particularly molecules with larger kinetic diameters. Therefore, physical aging among PIM-1 membranes can limit the diffusion of CH_4 (3.8 Å) to a greater extent than CO_2 (3.3 Å), and thus enhance the CO_2/CH_4 selectivity, as observed for the prepared TFCs. Also, as aforementioned, physical aging rate is faster in thin films [19, 41]. In this study, a reduction in CO_2 permeability of about 47% was observed for the freestanding PIM-1 membrane after 230 days (as compared to a much faster and higher reduction, 63%, for the TFC in only 16 days). In most studies, differences in aging performance of PIM-1 can be linked to changes in the polymer structure, different storage conditions, thickness of the polymer film, and post-treatments done [40].

Fabricated TFCs with Cardo-PIM-1 were able to mitigate the physical aging as compared to the base PIM-1 thin films. In the plots in Fig. 7(a) and (b) it can be observed that the drop in CO_2 permeance takes place more rapidly up to 37 days and slows down quite significantly thereafter for all the TFCs at different cardo loadings. Noteworthy is the influence of the bis(phenyl)fluorene substituent on the redistribution of polymer chains during aging; after 365 days, TFC-5.0 Cardo-PIM-1 underwent the lowest loss of CO_2 permeance (59%), from 12632 ± 866 to 5193 ± 529 GPU. CO_2/CH_4 selectivities increased significantly in all cases (Fig. 7 (c)) due to the more effective packing of the polymer, and thus an increased diffusivity-selectivity of the membranes. Greater increases were observed for membranes that underwent larger gas permeance loss. The available free space was smaller as polymer chains were able to relax to a greater extent, affecting more the permeance of bigger gas molecules, in this case CH_4, and so the CO_2/CH_4 selectivity for the purely PIM-1 TFC and the TFC containing 1 wt% of cardo reached values of c.a. 40. The 365-day-aged TFC containing 5 wt% cardo reached a selectivity of 26.01 ± 5.84. It is therefore suggested that the Cardo-PIM-1 increased the polymer rigidity by moderately freezing the polymer chains due to strong interactions between the bis(phenyl)fluorine and the PIM-1 chains; a semi-interpenetrating polymer network could have been formed, which prevented molecular rearrangement.

Several papers have reported the incorporation of fillers into PIM-1 polymeric membranes for gas processes, most of them being free-standing thick membranes [43,47–50] and very few dealing with thin

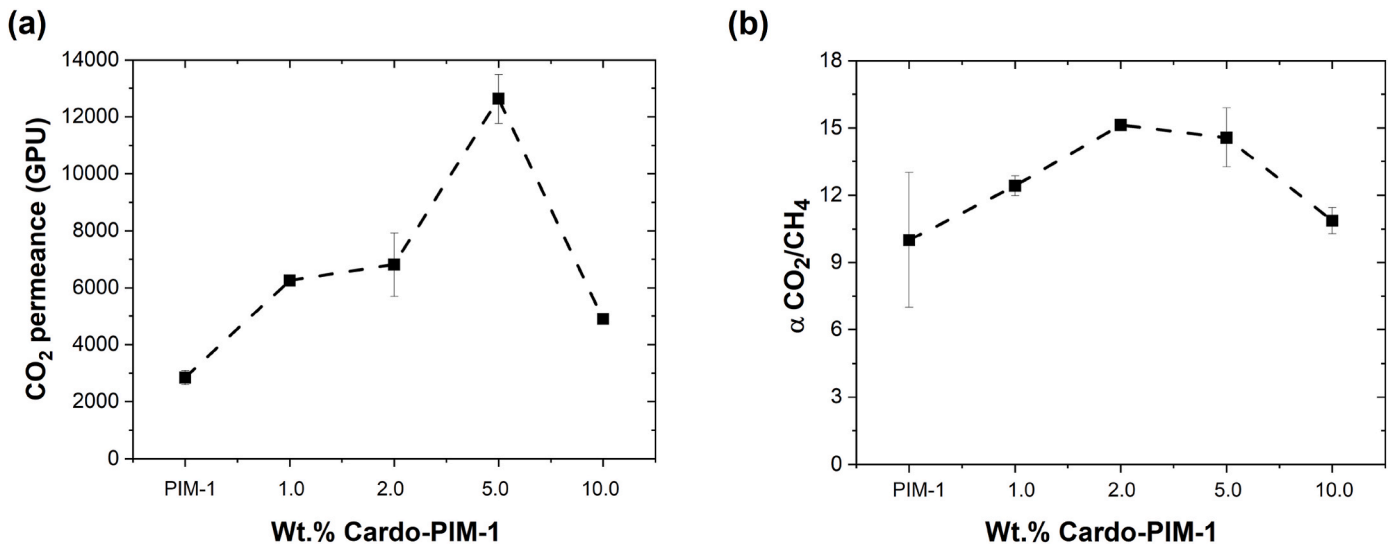

Fig. 6. CO_2 permeance (a) and CO_2/CH_4 ideal selectivity (b) of Cardo-PIM-1 based TFC membranes (dashed lines are used for guide purposes only).

Table 1
Gas permeability (*P*), diffusion (*D*) and solubility (*S*) coefficients, and ideal selectivity for fresh freestanding membranes.

Membrane	Membrane thickness (μm)	*P* (barrer)		*D* x10^7 (cm^2 s^{-1})		*S* x 10^3 (cm^3(STP) cm^{-3} $cmHg^{-1}$)		Ideal Sel CO_2/CH_4	Diffusivity selectivity	Solubility selectivity
		CO_2	CH_4	CO_2	CH_4	CO_2	CH_4			
PIM-1	69	7714	608	11.72	5.26	658	116	12.68	2.2	5.7
1.0Cardo-PIM-1	85	12628	1510	17.26	9.21	732	164	8.36	1.9	4.5
2.0Cardo-PIM-1	88	14644	1692	20.45	9.58	716	177	8.66	2.1	4.1
5.0Cardo-PIM-1	85	15191	873	16.41	6.60	925	132	17.40	2.5	7.0
10.0Cardo-PIM-1	80	10651	789	17.0	5.85	630	135	13.50	2.9	4.7

film membranes [40,51,52]. Our research group has recently reported the fabrication of thin film nanocomposite (TFN) membranes using nanosized UiO-66−NH_2/carboxylated PIM-1 (cPIM-1), which forms a stable three-dimensional (3D) network intertwining with the polymer chains [53]. The TFNs showed almost negligible aging with a CO_2 permeance value of 2504 GPU after 63 days from preparation. In a previous work we found that by adding 2D reduced holey graphene oxide (rHGO) nanosheets containing amine groups into thin films of PIM-1, aging was also prevented to a large extent at optimum loadings [41]. In this case, 1 wt% filler loading of rHGO-tris(4-aminophenyl) amine resulted in CO_2 permeance of 846 GPU after 1 year, which is near the CO_2 permeance of the fresh membranes tested right after preparation (1050 GPU). Moreover, the permeance doubled that of 1 year-aged purely PIM-1 thin film composite membranes (432 GPU). However, at lower filler concentrations of 0.1 wt%, the initial CO_2 permeance of the fresh TFN membrane was 3351 GPU, which after 1 year of aging dropped down to 604 GPU. In another approach to improve gas separation properties and aging, porous silica nanosheets (SN) functionalized by a sulfonic acid (S-SN) were added into PIM-1 [43]. The addition of 0.05 wt% resulted in 35% higher initial CO_2 permeance (3771 GPU) than the PIM-1 TFC (2778 GPU), but physical aging was prevented to a lower extent; after 28 days the CO_2 permeance of the aged PIM-1 TFC and TFN PIM/S-SN 0.05 wt%, dropped by 97% (81 GPU) and 87% (403 GPU), respectively.

Foster et al. [38] studied the effect of blending colloidal network rich PIM-1 samples with conventional di-substituted linear PIM-1 samples on gas performance and physical aging. Some blends cast into TFCs were able to arrest aging for up to one month. An optimised polymer synthesis, guided by these findings, produced PIM-1 polymer containing multiloop (3 small loops) structures and few chain ends (0−1 maximum) which when cast into TFCs exhibited excellent anti-aging behaviour and achieved a CO_2 permeance of 671 GPU after 120 days. Borisov et al. [52] fabricated TFCs with high CO_2 permeance (8010 GPU) and high CO_2/N_2 selectivity (35.8) owing to a strong synergistic effect due to the formation of a skinny edge layer between PIM-1 and cross linked poly [1-trimethylsily-1-propyne]. However, the 90 day-aged membranes underwent a severe drop in gas permeance (208 GPU), whereas maintaining approximately the same high selectivity.

Another study conducted by Bhavsar et al. [37] on highly permeable nanofillers (carbonized form of hypercrosslinked polystyrene, C-HCP) embedded into PIM-1 TFNs showed an excellent decrease in the rate of physical aging. After 90 days, very high filler loadings of C-HCP (60 wt %) resulted in CO_2 permeance of >9300 GPU, with a relatively low CO_2/N_2 selectivity value of 11. Liu et al. [51] reported PIM-1/MOF-based TFCs with high CO_2 permeance of 4660–7460 GPU and CO_2/N_2 selectivity of 26–33 with improved aging resistance, sustaining a steady CO_2 permeance of 900–1200 GPU after 8 weeks of aging. Another study by Kinoshita et al. [54] on PIM-1 TFNs using amine and nitro-functionalized polyhedral oligomeric silsesquioxane silica-based nanofillers showed a decrease of 90% of the initial CO_2 permeance after 30 days.

In our current work, the composite membrane containing 5 wt% of Cardo-PIM-1 shows a very good initial performance, reaching a CO_2 permeance of 12632 GPU. Moreover, this TFC undergoes aging only up to 37 days, where an attractive permeance of ca. 5000 GPU and a CO_2/CH_4 selectivity of 26 is obtained and retained from there on up to the testing period of 1 year. These permselectivity properties surpass those of any aged PIM-1 membrane ever reported. A comparison of the CO_2 permeance of the TFCs fabricated in this work with other thin film membranes data reported in the literature is shown in Table 2.

Fig. 8 illustrates the gas separation performance on a permeability-selectivity Robeson plot of the thin film membrane containing Cardo-PIM-1 with loadings 1, 2,5 and 10 wt% and the pristine PIM-1

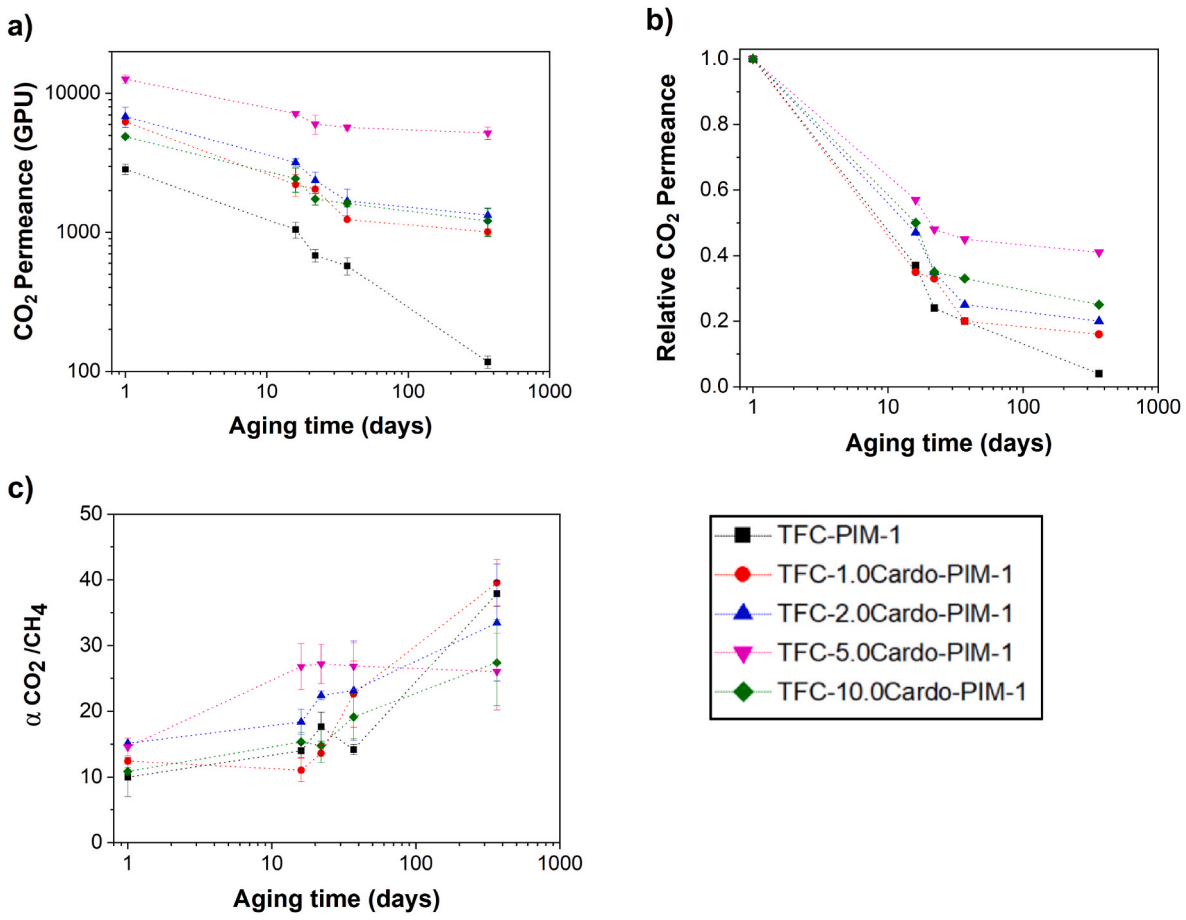

Fig. 7. Evaluation of membrane aging of PIM-1 TFC and TFC membranes containing Cardo-PIM-1 with loadings 1, 2, 5 and 10 wt% over 1 year. CO_2 permeance (a), relative CO_2 permeance (b) and ideal CO_2/CH_4 selectivity (c). At least two membranes of each type were tested and the error bars correspond to the standard deviation. 1 GPU = 10^{-6} cm^3 [STP] cm^{-2} s^{-1} $cmHg^{-1}$. Dashed lines are used for guide purposes only.

membrane. Data of freshly prepared membranes and aged ones over a period of a year are displayed with the 2008 Robeson [7] and the 2019 Jansen/McKeown [55] upper-bounds. It is observed that the incorporation of Cardo-PIM-1 into the polymer matrix is a promising strategy to surpass the 2008 upper bound. Upon aging, the composite membranes follow the upper bound towards higher CO_2/CH_4 selectivity and lower CO_2 permeance, as expected. Among all membranes, TFC-5.0Cardo-PIM-1 shows the best performance as it is closer to the 2019 upper bound. It is worth noting that after 365 days, TFCs with the cardo polymer displayed a lower permeance drop than pristine PIM-1.

Thick freestanding membranes incorporating Cardo-PIM-1 were also prepared and their gas separation performance for CO_2/CH_4 mixtures investigated and compared to pristine PIM-1 membranes. Results are collected in Table S3 and plotted in Figs. S11 and S12. The gas separation performance showed similar tendencies to those of thin films, i.e. higher permeability without sacrificing CO_2/CH_4 selectivity. 5.0 wt% Cardo-PIM-1 reached an initial CO_2 permeability of (15187 ± 789 barrer), outperforming the neat PIM-1 membrane with almost half of the CO_2 permeability (7256 ± 320 barrer). The aging behavior was also investigated up to 230 days and, as expected, the relative CO_2 permeability was always higher in freestanding membranes, with TFCs only capable of reaching maximum values after 1 year of c.a. 0.4 for the optimum membrane with 5 wt% Cardo-PIM-1. On the contrary the 10 wt % Cardo-PIM-1 showed a value of 0.77 after 230 days. it is worth noting that the permeance decrease plateaus after 37 days of aging for thin film membranes, while it takes relatively longer for freestanding ones (>100 days). This confirms faster aging in thin films. When looking at the CO_2/CH_4 selectivity vs CO_2 permeability plot for the freestanding membranes (Fig. S12), it is evident that aging moves performance towards higher permeability and selectivity. After 230 days, these values are all above the 2008 Robeson upper bound and converge in c.a. 10000 barrer of CO_2 permeability and a CO_2/CH_4 selectivity of 13.

To evaluate more about the performance of the Cardo-PIM-1in the membranes, a time-lag apparatus was used for single gas permeation measurements of fresh membranes. The highly preferred transport mechanism for gas permeation in polymer membranes is the solution-diffusion mechanism. Solubility (*S*) and diffusion (*D*) coefficients of PIM-1 and Cardo-PIM-1-based PIM-1 membranes were calculated using pure gas measurements from a constant volume instrument as shown in Table 1. *S* and *D* values obtained from PIM-1 membranes are comparable to the values stated by Budd et al. [11], and the gas permeability and selectivity very similar to those obtained with mixed gases (Table S3). Since CO_2 has a smaller kinetic diameter and higher polarity, the calculated *D* and *S* values for this gas are both higher than those for CH_4. It is important to note that the CO_2 permeability obtained for all freestanding membranes containing the cardo polymer is higher than the permeability of pure PIM-1, as previously observed in the results of the mixed gas testing and in agreement with higher permeances in the TFCs. The more rapid diffusion of CO_2 across the membranes when optimum loadings of Cardo-PIM-1 are added suggests increased free volume. Indeed, Cardo-PIM-1 has numerous, bigger micropores due to the inefficient packing of the polymer as a consequence of its more rigid and contorted architecture. This leads to a more permeable overall structure for both CO_2 and CH_4 gas molecules, which results in very slim differences in diffusivity selectivity. However, for the membrane with 5 wt % of Cardo-PIM-1, sorption of CO_2 increases quite considerably as

Table 2
Comparison of CO_2 permeance of the TFC cardo-based membranes fabricated in this work with other TFC data reported in the literature.

Membrane Name	Aging (days)	CO_2 Permeance (GPU)	CO_2/CH_4 Selectivity	Reference
TFC-PIM-1	1	2850	10	This work
	365	117	37.9	
TFC-1.0Cardo-PIM-1	1	6256	12.4	
	365	1002	39.5	
TFC-2.0Cardo-PIM-1	1	6817	15.1	
	365	1334	33.5	
TFC-5.0Cardo-PIM-1	1	12632	14.6	
	365	5193	26	
TFC PIM-1 (2 μm)	1	4642	–	[38]
	120	671	–	
TFC#1 PIM-1(0.29 μm) + PTMSP(2.3 μm)	1	8010	–	[52]
	98	208	–	
TFC-PIM-1 (2.08 μm)	1	3331	–	[37]
	90	388	–	
60% C-HCP-PIM-1 (8.05 μm)	1	27530	–	
	90	9379	–	
40% HCP-PIM-1 (1.38 μm)	1	10028	–	
	90	556	–	
60% HCP-PIM-1 (6.32 μm)	1	21627	–	
	90	6839	–	
TFC PIM-1 (2.5 μm)	1	2778	6.3	[43]
	28	81	6.1	
TFN-S-SN 0.05- PIM-1 (2.5 μm)	1	3771	8.7	
	28	403	5.5	
TFN-S-SN 0.25	1	2755	6.5	
	28	393	7.7	
TFC-PIM-1 (2.04 μm)	1	4599	13	[53]
	28	1331	12.1	
TFN-UiO-66−NH_2/carboxylated PIM-1 (2.05 μm)	1	2664	19	
	63	2504	23.8	
TFC-PIM-1 (2.5 μm)	1	2403	8.7	[54]
TFN POSS 5% - PIM-1 (2.5 μm)	1	2138	10.6	
TFC-PIM-1 (200 nm)	1	16917	8.2	
TFN POSS 5% - PIM-1 (200 nm)	1	13585	9.7	
TFC- PIM-1	1	4320	–	[51]
	60	490	–	
10 wt% MOF-74-Ni -PIM-1	1	5018	–	
	60	1200	–	
10 wt% NH_2-UiO-66 MOF-PIM-1	1	7460	–	
	60	900	–	
Metallic ion-crosslinked PIM-1 TFC	1	1058		[56]

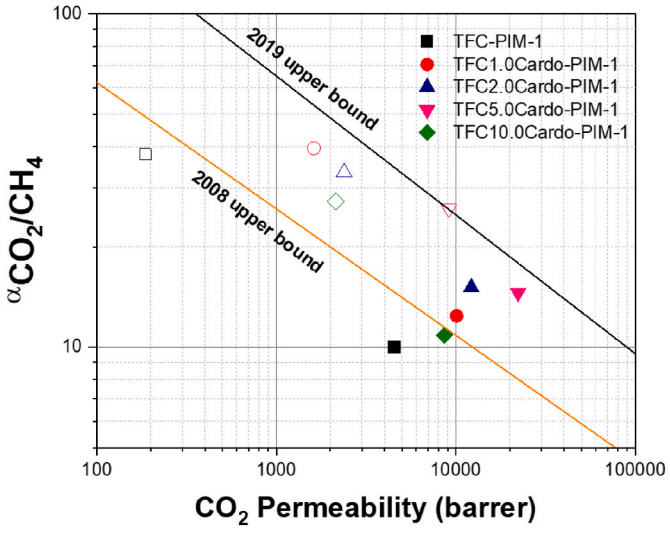

Fig. 8. Comparison of the CO_2/CH_4 separation performance of a PIM-1 TFC and the TFC membranes containing Cardo-PIM-1 in a CO_2/CH_4 selectivity vs CO_2 permeability plot with the 2008 Robeson [7] and 2019 Jansen/McKeown [55] upper-bounds. Membranes were tested at 25 °C under a transmembrane pressure of 1 bar. Filled and empty symbols represent the performance at day 1 and day 365, respectively. Membrane thickness values in the range of 1.4–1.7 μm were considered to convert permeance to permeability.

compared to pure PIM-1, and the solubility selectivity towards CO_2 increases from 5.7 (PIM-1) to 7 (5.0Cardo-PIM-1). The study by Sun et al. [31] confirmed that CO_2 sorption at 298 K of Cardo-PIM-1 is significantly higher than that of PIM-1. Bigger micropores have plenty of Langmuir adsorption sites saturated at a low pressure, which helps in enhancing the CO_2 solubility coefficient.

4. Conclusions

The effect of the incorporation of a colloidal network-rich Cardo-PIM-1 into a branched PIM-1 polymeric matrix on the CO_2/CH_4 separation performance was studied. Thin film composite (TFC) membranes of PIM-1 containing different loadings of Cardo-PIM-1 were tested and their physical aging behavior evaluated. After 1 year of aging, membranes with a loading of 5 wt% Cardo-PIM-1 obtained a 44 times higher CO_2 permeance compared to purely PIM-1 thin film composite membranes, 5193 ± 529 GPU and 117 ± 12 GPU, respectively. This impressively stable performance is attributed to the formation of a semi interpenetrating polymeric network between the dispersed colloidal network rich Cardo-PIM-1 and the heavily branched base PIM-1 polymer used in the blending process.

The effect of physical aging on the gas separation performance for several tens of micrometers thick membranes with Cardo-PIM-1 loadings of 1–10 wt% was also evaluated. The gas separation results obtained were similar to thin films, showing a higher CO_2/CH_4 selectivity as well as higher CO_2 permeability. 5 wt% Cardo-PIM-1 obtained an initial CO_2 permeability of 15187 ± 789 barrer. Thus, CO_2/CH_4

separation performance surpassed that of neat PIM-1 membranes. We showed that adding Cardo-PIM-1 led to higher diffusion and solubility coefficients, and enhanced the free volume. Therefore, the addition of Cardo-PIM-1 in freestanding membranes seems to be amongst the most efficient approaches for improving the gas separation performances of PIM-1-based membranes.

CRediT authorship contribution statement

Faiz Almansour: Writing – original draft, Investigation, Formal analysis, Conceptualization. **Andrew B. Foster:** Writing – review & editing, Investigation, Formal analysis. **Ahmed W. Ameen:** Methodology. **Sajjad Mohsenpour:** Methodology. **Peter M. Budd:** Writing – review & editing, Supervision, Resources. **Patricia Gorgojo:** Writing – review & editing, Supervision, Project administration, Funding acquisition, Conceptualization.

Declaration of competing interest

The authors declare that they have no known competing financial interests or personal relationships that could have appeared to influence the work reported in this paper.

Data availability

Data will be made available on request.

Acknowledgments

Faiz Almansour is grateful to the Department of Research & Development Centre, Saudi Aramco for funding and supporting his PhD studies. Patricia Gorgojo is grateful to her fellowship with reference RYC2019-027060-I funded by MCIN/AEI/10.13039/501100011033 and European Union NextGenerationEU/PRTR. Andrew B. Foster is grateful to EPSRC Programme Grant ep/v047078/1 "SynHiSel". We thank Dr. Jennifer Saunders and Mustafa Alshurafa for their assistance with some additional TGA and XRD analysis, respectively.

Appendix A. Supplementary data

Supplementary data to this article can be found online at https://doi.org/10.1016/j.memsci.2024.122652.

References

[1] K. Schoots, R. Rivera-Tinoco, G. Verbong, B. van der Zwaan, Historical variation in the capital costs of natural gas, carbon dioxide and hydrogen pipelines and implications for future infrastructure, Int. J. Greenh. Gas Control 5 (6) (2011) 1614–1623, https://doi.org/10.1016/j.ijggc.2011.09.008.
[2] R.W. Baker, K. Lokhandwala, Natural gas processing with membranes: an overview, Ind. Eng. Chem. Res. 47 (7) (2008) 2109–2121, https://doi.org/10.1021/ie071083w.
[3] Y. Xiao, B.T. Low, S.S. Hosseini, T.S. Chung, D.R. Paul, The strategies of molecular architecture and modification of polyimide-based membranes for CO_2 removal from natural gas—a review, Prog. Polym. Sci. 34 (6) (2009) 561–580, https://doi.org/10.1016/j.progpolymsci.2008.12.004.
[4] A.J. Kidnay, A.J. Kidnay, W.R. Parrish, D.G. McCartney, Fundamentals of Natural Gas Processing, second ed., CRC Press. Taylor & Francis Group, Boca Raton, 2011.
[5] W.F.J. Burgers, P.S. Northrop, H.S. Kheshgi, J.A. Valencia, Worldwide development potential for sour gas, Energy Proc. 4 (2011) 2178–2184, https://doi.org/10.1016/j.egypro.2011.02.104.
[6] P. Bernardo, E. Drioli, G. Golemme, Membrane gas separation: a review/state of the art, Ind. Eng. Chem. Res. 48 (10) (2009) 4638–4663, https://doi.org/10.1021/ie8019032.
[7] L.M. Robeson, The upper bound revisited, J. Membr. Sci. 320 (1) (2008) 390–400, https://doi.org/10.1016/j.memsci.2008.04.030.
[8] P.M. Budd, B.S. Ghanem, S. Makhseed, N.B. McKeown, K.J. Msayib, C. E. Tattershall, Polymers of intrinsic microporosity (PIMs): robust, solution-processable, organic nanoporous materials, Chem. Commun. (2) (2004) 230–231, https://doi.org/10.1039/B311764B.
[9] P.M. Budd, N.B. McKeown, D. Fritsch, Free volume and intrinsic microporosity in polymers, J. Mater. Chem. 15 (20) (2005) 1977–1986, https://doi.org/10.1039/B417402J.
[10] P.M. Budd, N.B. McKeown, D. Fritsch, Polymers of intrinsic microporosity (PIMs): high free volume polymers for membrane applications, Macromol. Symp. 245–246 (1) (2006) 403–405, https://doi.org/10.1002/masy.200651356.
[11] P.M. Budd, N.B. McKeown, B.S. Ghanem, K.J. Msayib, D. Fritsch, L. Starannikova, N. Belov, O. Sanfirova, Y. Yampolskii, V. Shantarovich, Gas permeation parameters and other physicochemical properties of a polymer of intrinsic microporosity: polybenzodioxane PIM-1, J. Membr. Sci. 325 (2) (2008) 851–860, https://doi.org/10.1016/j.memsci.2008.09.010.
[12] M.M. Merrick, R. Sujanani, B.D. Freeman, Glassy polymers: historical findings, membrane applications, and unresolved questions regarding physical aging, Polymer 211 (2020) 123176, https://doi.org/10.1016/j.polymer.2020.123176.
[13] J.H. Kim, W.J. Koros, D.R. Paul, Physical aging of thin 6FDA-based polyimide membranes containing carboxyl acid groups. Part II. Optical properties, Polymer 47 (9) (2006) 3104–3111, https://doi.org/10.1016/j.polymer.2006.02.079.
[14] R.R. Tiwari, J. Jin, B.D. Freeman, D.R. Paul, Physical aging, CO_2 sorption and plasticization in thin films of polymer with intrinsic microporosity (PIM-1), J. Membr. Sci. 537 (2017) 362–371, https://doi.org/10.1016/j.memsci.2017.04.069.
[15] Y. Huang, D.R. Paul, Effect of temperature on physical aging of thin glassy polymer films, Macromolecules 38 (24) (2005) 10148–10154, https://doi.org/10.1021/ma051284g.
[16] P. Bernardo, F. Bazzarelli, F. Tasselli, G. Clarizia, C.R. Mason, L. Maynard-Atem, P. M. Budd, M. Lanč, K. Pilnáček, O. Vopička, K. Friess, D. Fritsch, Y.P. Yampolskii, V. Shantarovich, J.C. Jansen, Effect of physical aging on the gas transport and sorption in PIM-1 membranes, Polymer 113 (2017) 283–294, https://doi.org/10.1016/j.polymer.2016.10.040.
[17] Y. Huang, D.R. Paul, Physical aging of thin glassy polymer films monitored by gas permeability, Polymer 45 (25) (2004) 8377–8393, https://doi.org/10.1016/j.polymer.2004.10.019.
[18] R.R. Tiwari, Z.P. Smith, H. Lin, B.D. Freeman, D.R. Paul, Gas permeation in thin films of "high free-volume" glassy perfluoropolymers: Part I, Physical aging, Polymer 55 (22) (2014) 5788–5800, https://doi.org/10.1016/j.polymer.2014.09.022.
[19] S. Harms, K. Rätzke, F. Faupel, N. Chaukura, P.M. Budd, W. Egger, L. Ravelli, Aging and free volume in a polymer of intrinsic microporosity (PIM-1), J. Adhes. 88 (7) (2012) 608–619, https://doi.org/10.1080/00218464.2012.682902.
[20] G. Maier, Gas separation with polymer membranes, Angew. Chem. Int. Ed. 37 (21) (1998) 2960–2974, https://doi.org/10.1002/(SICI)1521-3773(19981116)37:21<2960::AID-ANIE2960>3.0.CO;2-5.
[21] G. Chen, X. Zhang, S. Zhang, T. Chen, Y. Wu, Synthesis, properties, and gas permeation performance of cardo poly(arylene ether sulfone)s containing phthalimide side groups, J. Appl. Polym. Sci. 106 (4) (2007) 2808–2816, https://doi.org/10.1002/app.26930.
[22] Z. Xu, C. Dannenberg, J. Springer, S. Banerjee, G. Maier, Gas separation properties of polymers containing fluorene moieties, Chem. Mater. 14 (8) (2002) 3271–3276, https://doi.org/10.1021/cm0112789.
[23] Y. Lu, J. Hao, L. Li, J. Song, G. Xiao, H. Zhao, Z. Hu, T. Wang, Preparation and gas transport properties of thermally induced rigid membranes of copolyimide containing cardo moieties, React. Funct. Polym. 119 (2017) 134–144, https://doi.org/10.1016/j.reactfunctpolym.2017.08.013.
[24] S. Kazama, T. Teramoto, K. Haraya, Carbon dioxide and nitrogen transport properties of bis(phenyl)fluorene-based cardo polymer membranes, J. Membr. Sci. 207 (1) (2002) 91–104, https://doi.org/10.1016/S0376-7388(02)00112-6.
[25] C. Zhang, Synthesis and characterization of bis(phenyl)fluorene-based cardo polyimide membranes for H_2/CH_4 separation, J. Mater. Sci. 54 (14) (2019) 10560–10569, https://doi.org/10.1007/s10853-019-03609-2.
[26] G.O. Yahaya, I. Mokhtari, A.A. Alghannam, S.-H. Choi, H. Maab, A.A. Bahamdan, Cardo-type random co-polyimide membranes for high pressure pure and mixed sour gas feed separations, J. Membr. Sci. 550 (2018) 526–535, https://doi.org/10.1016/j.memsci.2017.10.063.
[27] S. Ghosh, S. Banerjee, Fluorinated poly(arylene ether)s with aliphatic chain appended cardo moiety: synthesis and gas transport properties, J. Membr. Sci. 470 (2014) 535–546, https://doi.org/10.1016/j.memsci.2014.07.052.
[28] C. Camacho-Zuñiga, F.A. Ruiz-Treviño, M.G. Zolotukhin, L.F. del Castillo, J. Guzman, J. Chavez, G. Torres, N.G. Gileva, E.A. Sedova, Gas transport properties of new aromatic cardo poly(aryl ether ketone)s, J. Membr. Sci. 283 (1) (2006) 393–398, https://doi.org/10.1016/j.memsci.2006.07.013.
[29] M. Carta, M. Croad, J.C. Jansen, P. Bernardo, G. Clarizia, N.B. McKeown, Synthesis of cardo-polymers using Tröger's base formation, Polym. Chem. 5 (18) (2014) 5255–5261, https://doi.org/10.1039/C4PY00607K.
[30] B.S. Ghanem, N.B. McKeown, P.M. Budd, D. Fritsch, Polymers of intrinsic microporosity derived from bis(phenazyl) monomers, Macromolecules 41 (5) (2008) 1640–1646, https://doi.org/10.1021/ma071846r.
[31] H. Sun, W. Gao, Y. Zhang, X. Cao, S. Bao, P. Li, Z. Kang, Q.J. Niu, Bis(phenyl) fluorene-based polymer of intrinsic microporosity/functionalized multi-walled carbon nanotubes mixed matrix membranes for enhanced CO_2 separation performance, React. Funct. Polym. 147 (2020) 104465, https://doi.org/10.1016/j.reactfunctpolym.2019.104465.
[32] L. Hao, P. Li, T.-S. Chung, PIM-1 as an organic filler to enhance the gas separation performance of Ultem polyetherimide, J. Membr. Sci. 453 (2014) 614–623, https://doi.org/10.1016/j.memsci.2013.11.045.
[33] W.F. Yong, F.Y. Li, Y.C. Xiao, P. Li, K.P. Pramoda, Y.W. Tong, T.S. Chung, Molecular engineering of PIM-1/Matrimid blend membranes for gas separation,

J. Membr. Sci. 407–408 (2012) 47–57, https://doi.org/10.1016/j.memsci.2012.03.038.
[34] M. Tamaddondar, A.B. Foster, J.M. Luque-Alled, K.J. Msayib, M. Carta, S. Sorribas, P. Gorgojo, N.B. McKeown, P.M. Budd, Intrinsically microporous polymer nanosheets for high-performance gas separation membranes, Macromol. Rapid Commun. 41 (2) (2020) 1900572, https://doi.org/10.1002/marc.201900572.
[35] L. Gao, M. Alberto, P. Gorgojo, G. Szekely, P.M. Budd, High-flux PIM-1/PVDF thin film composite membranes for 1-butanol/water pervaporation, J. Membr. Sci. 529 (2017) 207–214, https://doi.org/10.1016/j.memsci.2017.02.008.
[36] A.W. Ameen, J. Ji, M. Tamaddondar, S. Moshenpour, A.B. Foster, X. Fan, P. M. Budd, D. Mattia, P. Gorgojo, 2D boron nitride nanosheets in PIM-1 membranes for CO_2/CH_4 separation, J. Membr. Sci. 636 (2021) 119527, https://doi.org/10.1016/j.memsci.2021.119527.
[37] R.S. Bhavsar, T. Mitra, D.J. Adams, A.I. Cooper, P.M. Budd, Ultrahigh-permeance PIM-1 based thin film nanocomposite membranes on PAN supports for CO_2 separation, J. Membr. Sci. 564 (2018) 878–886, https://doi.org/10.1016/j.memsci.2018.07.089.
[38] A.B. Foster, J.L. Beal, M. Tamaddondar, J.M. Luque-Alled, B. Robertson, M. Mathias, P. Gorgojo, P.M. Budd, Importance of small loops within PIM-1 topology on gas separation selectivity in thin film composite membranes, J. Mater. Chem. A 9 (38) (2021) 21807–21823, https://doi.org/10.1039/D1TA03712A.
[39] S. Aloraini, M. Mathias, J. Crone, K. Bryce, M. Yu, R.A. Kirk, M.Z. Ahmad, E. D. Asuquo, S. Rico-Martínez, A.V. Volkov, A.B. Foster, P.M. Budd, Crosslinking of branched PIM-1 and PIM-Py membranes for recovery of toluene from dimethyl sulfoxide by pervaporation, ACS Appl. Polym. Mater. 5 (2) (2023) 1145–1158, https://doi.org/10.1021/acsapm.2c01600.
[40] A.B. Foster, M. Tamaddondar, J.M. Luque-Alled, W.J. Harrison, Z. Li, P. Gorgojo, P. M. Budd, Understanding the topology of the polymer of intrinsic microporosity PIM-1: cyclics, tadpoles, and network structures and their impact on membrane performance, Macromolecules 53 (2) (2020) 569–583, https://doi.org/10.1021/acs.macromol.9b02185.
[41] F. Almansour, M. Alberto, A.B. Foster, S. Mohsenpour, P.M. Budd, P. Gorgojo, Thin film nanocomposite membranes of superglassy PIM-1 and amine-functionalised 2D fillers for gas separation, J. Mater. Chem. A 10 (43) (2022) 23341–23351, https://doi.org/10.1039/D2TA06339E.
[42] C.N. Cascaval, D. Rosu, L. Rosu, C. Ciobanu, Thermal degradation of semi-interpenetrating polymer networks based on polyurethane and epoxy maleate of bisphenol A, Polym. Test. 22 (1) (2003) 45–49, https://doi.org/10.1016/S0142-9418(02)00047-8.
[43] S. Mohsenpour, Z. Guo, F. Almansour, S.M. Holmes, P.M. Budd, P. Gorgojo, Porous silica nanosheets in PIM-1 membranes for CO_2 separation, J. Membr. Sci. 661 (2022) 120889, https://doi.org/10.1016/j.memsci.2022.120889.
[44] T.-S. Chung, L.Y. Jiang, Y. Li, S. Kulprathipanja, Mixed matrix membranes (MMMs) comprising organic polymers with dispersed inorganic fillers for gas separation, Prog. Polym. Sci. 32 (4) (2007) 483–507, https://doi.org/10.1016/j.progpolymsci.2007.01.008.
[45] D. Şen, H. Kalıpçılar, L. Yilmaz, Development of polycarbonate based zeolite 4A filled mixed matrix gas separation membranes, J. Membr. Sci. 303 (1) (2007) 194–203, https://doi.org/10.1016/j.memsci.2007.07.010.
[46] R. Swaidan, B. Ghanem, E. Litwiller, I. Pinnau, Physical aging, plasticization and their effects on gas permeation in “rigid” polymers of intrinsic microporosity, Macromolecules 48 (18) (2015) 6553–6561, https://doi.org/10.1021/acs.macromol.5b01581.
[47] C.G. Bezzu, M. Carta, A. Tonkins, J.C. Jansen, P. Bernardo, F. Bazzarelli, N. B. McKeown, A spirobifluorene-based polymer of intrinsic microporosity with improved performance for gas separation, Adv. Mater. 24 (44) (2012) 5930–5933, https://doi.org/10.1002/adma.201202393.
[48] B.S. Ghanem, R. Swaidan, E. Litwiller, I. Pinnau, Ultra-microporous triptycene-based polyimide membranes for high-performance gas separation, Adv. Mater. 26 (22) (2014) 3688–3692, https://doi.org/10.1002/adma.201306229.
[49] C.H. Lau, K. Konstas, A.W. Thornton, A.C.Y. Liu, S. Mudie, D.F. Kennedy, S. C. Howard, A.J. Hill, M.R. Hill, Gas-separation membranes loaded with porous aromatic frameworks that improve with age, Angew. Chem. Int. Ed. 54 (9) (2015) 2669–2673, https://doi.org/10.1002/anie.201410684.
[50] S. Mohsenpour, A.W. Ameen, S. Leaper, C. Skuse, F. Almansour, P.M. Budd, P. Gorgojo, PIM-1 membranes containing POSS - graphene oxide for CO_2 separation, Sep. Purif. Technol. 298 (2022) 121447, https://doi.org/10.1016/j.seppur.2022.121447.
[51] M. Liu, M.D. Nothling, P.A. Webley, J. Jin, Q. Fu, G.G. Qiao, High-throughput CO_2 capture using PIM-1@MOF based thin film composite membranes, Chem. Eng. J. 396 (2020) 125328, https://doi.org/10.1016/j.cej.2020.125328.
[52] I. Borisov, D. Bakhtin, Jose M. Luque-Alled, A. Rybakova, V. Makarova, A.B. Foster, W.J. Harrison, V. Volkov, V. Polevaya, P. Gorgojo, E. Prestat, P.M. Budd, A. Volkov, Synergistic enhancement of gas selectivity in thin film composite membranes of PIM-1, J. Mater. Chem. A 7 (11) (2019) 6417–6430, https://doi.org/10.1039/C8TA10691F.
[53] B. Qiu, M. Yu, J.M. Luque-Alled, S. Ding, A.B. Foster, P.M. Budd, X. Fan, P. Gorgojo, High gas permeability in aged superglassy membranes with nanosized UiO-66−NH_2/cPIM-1 network fillers, Angew. Chem. Int. Ed. 63 (1) (2024) e202316356, https://doi.org/10.1002/anie.202316356.
[54] Y. Kinoshita, K. Wakimoto, A.H. Gibbons, A.P. Isfahani, H. Kusuda, E. Sivaniah, B. Ghalei, Enhanced PIM-1 membrane gas separation selectivity through efficient dispersion of functionalized POSS fillers, J. Membr. Sci. 539 (2017) 178–186, https://doi.org/10.1016/j.memsci.2017.05.072.
[55] B. Comesaña-Gándara, J. Chen, C.G. Bezzu, M. Carta, I. Rose, M.-C. Ferrari, E. Esposito, A. Fuoco, J.C. Jansen, N.B. McKeown, Redefining the Robeson upper bounds for CO_2/CH_4 and CO_2/N_2 separations using a series of ultrapermeable benzotriptycene-based polymers of intrinsic microporosity, Energy Environ. Sci. 12 (9) (2019) 2733–2740, https://doi.org/10.1039/C9EE01384A.
[56] H. Zhao, L. Feng, X. Ding, X. Tan, Y. Zhang, Gas permeation properties of a metallic ion-cross-linked PIM-1 thin-film composite membrane supported on a UV-cross-linked porous substrate, Chin. J. Chem. Eng. 26 (12) (2018) 2477–2486, https://doi.org/10.1016/j.cjche.2018.03.009.